Misalignment Fault Detection in Dual-rotor System Based on Time Frequency Techniques

Nan-fei Wang, Dong-xiang Jiang*, Te Han
State Key Laboratory of Control and Simulation of Power System and Generation Equipment,
Department of Thermal Engineering,
Tsinghua University, Beijing, 100084, China

Abstract. In order to improve the energy efficiency and compact structure, the dual-rotor structure including low-pressure rotor and high-pressure rotor has been widely used in aero-engine. Misalignment is one of the most common faults in dual-rotor system, which will causes malfunctions. It is a significant task for rotor dynamics personnel to monitor and defect faults in dual-rotor system. In the paper, the dual-rotor vibration signals are applied to solve the fault identification problem by utilizing time frequency techniques. Numerical simulations are carried out through finite element analysis of dual-rotor system with misalignment fault. Two signal processing tools namely Short Time Fourier Transform (STFT) and Continuous Wavelet Transform are used to detect the misalignment fault and compared to evaluate their diagnosis performance. The effect of addition of Signal to Noise (SNR) on three frequency techniques is presented. Experiments are carried out to obtain the vibration data of dual-rotor test rig and the results from the work show that the technique can be used for the monitoring of misalignment, which will have applications in the condition monitoring and maintenance of various types of rotating machinery.

1 Introduction

Misalignment is a situation in which the input shaft and the output shaft are not in the identical centreline. It is very challenging to attain a perfectly aligned condition between two shafts in industrial environment. Even if an accurate alignment is secured, it cannot not be continued for a long duration due to many external effects, like base foundation disturbance [1, 2]. Shaft misalignment is a frequently encountered fault observed in large rotor bearing systems like steam turbine shafts, gas turbines shafts and aircraft rotating components, and it is a significant source of vibration. High levels of misalignment may lead to fatigue cracks or rotor to stator rubbing. Therefore, misalignment detection and monitoring is an important objective for successful operation in the industrial scenario. Precision detection of shaft misalignment faults can cut the operation cost and facilitate long and safe operation.

Due to the complexity of the misalignment fault, many comprehensive researches on the misalignment experiments and misalignment dynamics mechanism have been carried out based on the vibration information of a misalignment rotor system. The vibration response of the rotor provides knowledge on operating conditions that are connected to the fault characteristics. However, due to the confusing spectral characteristics of vibration, vibration based misalignment detection lead to less reliability [1]. It was practically proved that vibration magnitude varies significantly at $2\times$ and $4\times$ frequencies of operating frequency of the rotating member as the misalignment increases [3]. Also it is reported that the frequencies of forces and moments from misaligned shafts are even multiples of the operating speed of the motor [2, 4]. Analysis of other faults with analytical models of rotating systems reported by Hamzaoui et al. [5] also indicated that misaligned shafts generates vibrations such that the magnitude of the $2\times$ operating harmonic frequency component is sensitive to the fault. Sekhar and Prabhu [6] analyzed shaft misalignment in rotor bearing system with a flexible coupling using higher-order finite element model by applying theoretically modeled forces and moments. The effect of harmonic and flexural mode shapes on vibration magnitude is reported. Lee and Lee [7] introduced a dynamic model for shaft misalignment in a rotor-bearing system with roller bearing connected by flexible coupling. A model-based evaluation of defects in frequency domain was reported by [8-10]. Sinha et al. [11] introduced a technique to diagnose the shaft misalignment from a shutdown data in which the shaft misalignment at couplings is assumed to developed steady forces and moments.

In the above literature, the researchers pay more attention to the single-rotor system, which has significant difference with actual aero-engine. The arrangement of dual rotors is a common configuration utilized in practise to obtain the higher thrust to weight ratio [12]. Up to now, the effects of misalignment on the dynamic responses of the dual-rotor system have not been investigated in detail. Hence, it is of crucial importance to investigate the

misalignment fault mechanism of dual-rotor system for safe and steady running of aero-engine.

The objective of the study is to detect misalignment faults existing in a dual-rotor system. In the study both simulations and experimental investigations of misalignment fault detection are considered. Use of CWT algorithm is highlighted along with a comparative study using the STFT approach. The vibration equations of dual-rotor system are computed by numerical method and the results are investigated by the time waveform, frequency spectrum and time-frequency maps. Besides, the experiments with unbalance-misalignment is carried out on a dual-rotor test rig and the vibration displacement signals of the low pressure rotor are analyzed in detail.

2 Overview of time frequency techniques

In the following sub-sections, the time frequency techniques used in the present study for fault diagnosis are discussed briefly. Using time-frequency techniques, a view on rotor fault diagnosis is reported by Feng et al. [13] and Yan et al. [14].

2.1 Short Time Fourier Transform (STFT)

STFT is also called windowed Fourier transform, it is used to examine the features of a response with respect to time. For a vibration response $y(t)$, with $w(\tau - t)$ as the window function centered at time t, the response $y(t)$ using this window function is $y(t)w(\tau - t)$. Shifting the function $w(\tau - t)$ along the time axis of the response and employing the Fourier analysis to every window components lead to the following integral [13]:

$$S_y(t,f) = \int_{-\infty}^{+\infty} y(\tau)g(\tau - t)\, e^{-2\pi f \tau} d \qquad (1)$$

2.2 Continuous Wavelet Transform (CWT)

Continuous Wavelet Transform uses basis functions with translation and dilation parameters instead of simple complex exponentials unlike Fourier transform [13]. It adds a dilation parameter along with a time translation parameter to the analysis. Hence, it is best suited for time-frequency analysis, and is effective in analysing non-stationary signals like run-up vibration data of the rotor. CWT of a time signal $y(t)$ is obtained by solving the following convolution integral:

$$C_y(t,a) = \frac{1}{\sqrt{a}} \int_{-\infty}^{+\infty} y(\tau)\psi\left(\frac{\tau - t}{a}\right) d \qquad (2)$$

In the present work Complex Morlet (CMOR) wavelet function is chosen as the base wavelet

3 Simulation experiment

In order to evaluate the performance of STFT and CWT, a signal s that contains frequency components of f_1=500Hz and f_2=1000Hz was constructed. The specific expression of signal s is defined as follows:

$$s = \begin{cases} \sin(2\pi f_1 t) + \sin(2\pi f_2 t) \ (t \in [0, 0.256]) \\ s + 5 \ (t = 0.190) \\ s + 5 \ (t = 0.196) \end{cases} \qquad (3)$$

The time-frequency spectrum of STFT, time waveform and spectral analysis of the constructed signal are presented in Figure 1. The time-frequency spectrum of wavelet is illustrated in Figure 1. It can be observed from the expression and the time waveform of the signal that it has two peaks at $t = 0.190$ and $t = 0.196$, and two frequency components corresponding to f_1 and f_2 can be separated accurately. However, the time-frequency resolution of the STFT is fixed when the window function and its length are chosen. The continuous wavelet transform (CWT) is a well-developed tool employing wavelets as the basis to overcome the limitations of the STFT, adding a scale variable in addition to the time variable. Therefore, by comparing the time-frequency spectrum of Figure 1 and Figure 2, it can be found that the time-frequency map of CWT has better performance.

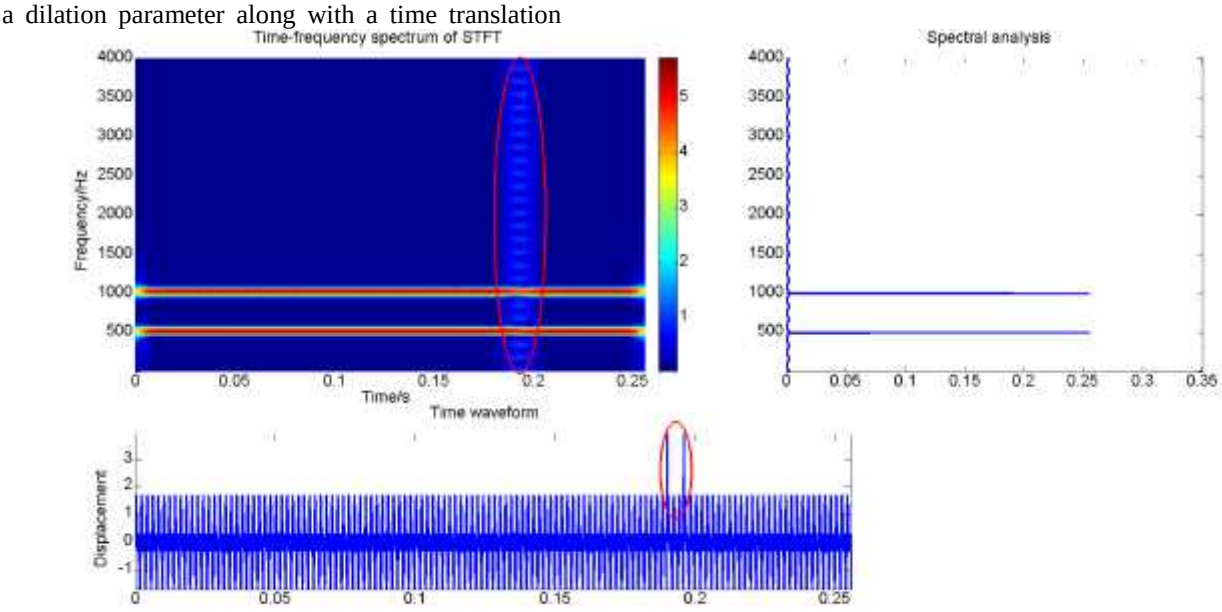

Figure 1 Time-frequency spectrum, time waveform and spectral analysis of the constructed signal

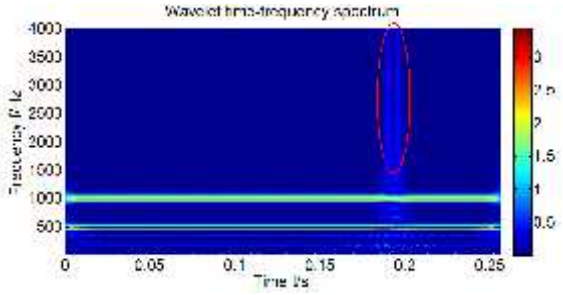

Figure 2 Time-frequency spectrum of wavelet

4 Dual-rotor system model with fault

The dual-rotor system with misalignment fault is shown in Figure 3, which consists of a low pressure rotor (rotor 1, lumped mass point 1 to 5) with a lower rotating speed and a high pressure rotor (rotor 2, lumped mass point 6 to 9) with a high rotating speed. There are four bearings included in the model, in which bearing 3 denotes the inter-shaft bearing. The disks 1-4, located, respectively at lumped mass points 2, 4, 7 and 9, represent the concentrations of low-pressure compressor disk, low-pressure turbine disk, high-pressure turbine disk and high-pressure compressor disk. The coupling misalignment fault including parallel and angular misalignment is modelled. It is assumed that the lumped masses at every lumped mass point are m_i $(i = 1 \cdots 9)$, the corresponding damping coefficients of which are c_i $(i = 1 \cdots 9)$, respectively. k_i $(i = 1 \cdots 7)$ are the stiffness coefficients of shaft segments, respectively. In order to research the dynamic characteristics of the dual-rotor model, the following assumptions are employed:

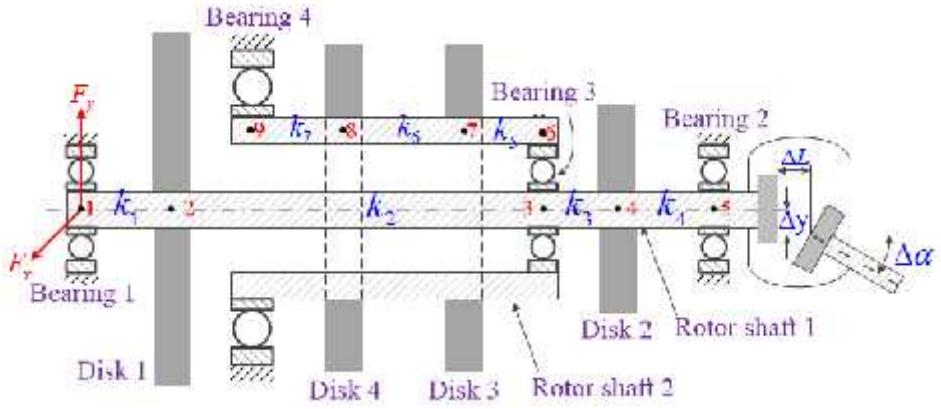

Figure 3 Mechanical model of the dual-rotor system

3.1 Misalignment modelling

The model in the study mainly considers the coupling integrated misalignment, which includes two cases of angle misalignment and parallel misalignment. When the master and slave rotor axis connected through the coupling exists misalignment, coupling housing is forced to make circular motion around its center by the limit of the two halve-coupling rotating around their respective axes. Its trajectory can be described by the following formulas:

$$\begin{cases} x = \Delta E\sin\theta & = \frac{1}{2}(\Delta y + \Delta L\tan(\Delta\alpha/2))\sin 2\theta \\ y = \Delta E & -\frac{1}{2}\Delta E = \frac{1}{2}(\Delta y + \Delta L\tan(\Delta\alpha/2))\cos 2\theta \end{cases} \quad (4)$$

where ΔE is the equivalent amount of misalignment, which is determined by the coupling spacing ΔL, parallel misalignment amount Δy and misalignment angle $\Delta\alpha$, $\Delta E = \Delta y + \Delta L \cdot \tan(\Delta\alpha/2)$.

Through Newton's second law of motion and acceleration of couplings can obtain equivalent misalignment force:

$$\begin{cases} F_x & = m_0 \cdot (\Delta y + \Delta L \cdot \tan(\Delta\alpha/2)) \cdot \omega_1^2 \cdot \sin(2\omega_1 t) \\ F_y & = m_0 \cdot (\Delta y + \Delta L \cdot \tan(\Delta\alpha/2)) \cdot \omega_1^2 \cdot \cos(2\omega_1 t) \end{cases} \quad (5)$$

where $\omega_1$is the rotating speed, m_0 denotes the mass of the coupling housing.

3.2 Equation of motion

Based on the above analysis and mechanical model of the dual-rotor system shown in Figure 3, using the principle of force equilibrium and Newton's law of motion, with the external forces exerted on the dual rotors that include the imbalance force, the bearing restoring force, viscous damping force and gravity, the system's governing equations of motion can be obtained

$$
\begin{cases}
m_1\ddot{x}_1 + c_1\dot{x}_1 + k_1(x_1 - x_2) = F_{x1} \\
m_1\ddot{y}_1 + c_1\dot{y}_1 + k_1(y_1 - y_2) = F_{y1} - m_1 g \\
m_2\ddot{x}_2 + c_2\dot{x}_2 + k_1(x_2 - x_1) + k_2(x_2 - x_3) = m_2 e_1\omega_1^2\cos(\omega_1 t) \\
m_2\ddot{y}_2 + c_2\dot{y}_2 + k_1(y_2 - y_1) + k_2(y_2 - y_3) = m_2 e_1\omega_1^2 \sin(\omega_1 t) - m_2 g \\
m_3\ddot{x}_3 + c_3\dot{x}_3 + k_2(x_3 - x_2) + k_3(x_3 - x_4) = -F_x \\
m_3\ddot{y}_3 + c_3\dot{y}_3 + k_2(y_3 - y_2) + k_3(y_3 - y_4) = -F_y \\
m_4\ddot{x}_4 + c_4\dot{x}_4 + k_3(x_4 - x_3) + k_4(x_4 - x_5) = m_4 e_2\omega_1^2\cos(\omega_1 t) \\
m_4\ddot{y}_4 + c_4\dot{y}_4 + k_3(y_4 - y_3) + k_4(y_4 - y_5) = m_4 e_2\omega_1^2 \sin(\omega_1 t) - m_4 g \\
m_5\ddot{x}_5 + c_5\dot{x}_5 + k_4(x_5 - x_4) = F_{x2} + F_x \\
m_5\ddot{y}_5 + c_5\dot{y}_5 + k_4(y_5 - y_4) = F_{y2} + F_y - m_5 g \\
m_6\ddot{x}_6 + c_6\dot{x}_6 + k_5(x_6 - x_7) = -F_x \\
m_6\ddot{y}_6 + c_6\dot{y}_6 + k_5(y_6 - y_7) = -F_{yh} - m_6 g \\
m_7\ddot{x}_7 + c_7\dot{x}_7 + k_5(x_7 - x_6) + k_6(x_7 - x_8) = m_7 e_3\omega_2^2\cos(\omega_2 t) + F_x \\
m_7\ddot{y}_7 + c_7\dot{y}_7 + k_5(y_7 - y_6) + k_6(y_7 - y_8) = m_7 e_3\omega_2^2 \sin(\omega_2 t) + F_y - m_7 g \\
m_8\ddot{x}_8 + c_8\dot{x}_8 + k_6(x_8 - x_7) + k_7(x_8 - x_9) = m_8 e_4\omega_2^2\cos(\omega_2 t) \\
m_8\ddot{y}_8 + c_8\dot{y}_8 + k_6(y_8 - y_7) + k_7(y_8 - y_9) = m_8 e_4\omega_2^2 \sin(\omega_2 t) - m_8 g \\
m_9\ddot{x}_9 + c_9\dot{x}_9 + k_7(x_9 - x_8) = F_{x4} \\
m_9\ddot{y}_9 + c_9\dot{y}_9 + k_7(y_9 - y_8) = F_{y4} - m_9 g
\end{cases}
\tag{6}
$$

where e_i $(i = 1 \cdots 4)$ are defined as the mass eccentricities of different disks, respectively; $(x_i, y_i)(i = 1 \cdots 9)$ denotes the vibration displacements of different lumped mass points, respectively; F_{x1} and F_{y1} represent the force components on the rotor from ith bearing $(i = 1,2,4)$, respectively; F_x and F_y are the force components exerted on the inner rotor due to misalignment faults.

It can be clearly observed from Figure 3 that (x_R, y_R) is (x_5, y_5), and (x_R, y_R) is (x_7, y_7). Therefore, the Equations (14)~(17) can be rewritten in a matrix form as

$$
\mathbf{M}\ddot{\boldsymbol{X}} + \mathbf{C}\dot{\boldsymbol{X}} + \boldsymbol{K} = \boldsymbol{F}(t) \tag{7}
$$

where $\boldsymbol{X} = \{x_1, y_1, \cdots x_9, y_9, x_w, y_w, x_b, y_b\}$ is the displacement vector corresponding to each mass. $\mathbf{M}$, $\mathbf{C}$ and $\boldsymbol{K}$ are the mass, damping and stiffness matrices, respectively. $\boldsymbol{F}(t)$ stands for the extra force vector.

5 Results and discussion

Based on the actual dual-rotor test rig, we pay more attention to co-rotation. In the case of $\omega_1 = 2000rr$, $\omega_2 = 3000rr$ $(\kappa = 1.5)$, lateral vibration plot and corresponding spectrum of lumped mass point 5 under unbalance-misalignment coupling faults are exhibited in Figure 4 and Figure 5 (e_2=5mm, $\Delta\alpha = \pi/18$, Δy = 5mm). It can be found from Figure 4 and Figure 5 that the rotational frequencies of inner and outer rotors and double frequency of inner rotor are very prominent, which is in accordance with literature [15]. Meanwhile, the CWT has better performance than STFT on extracting the fault characteristics.

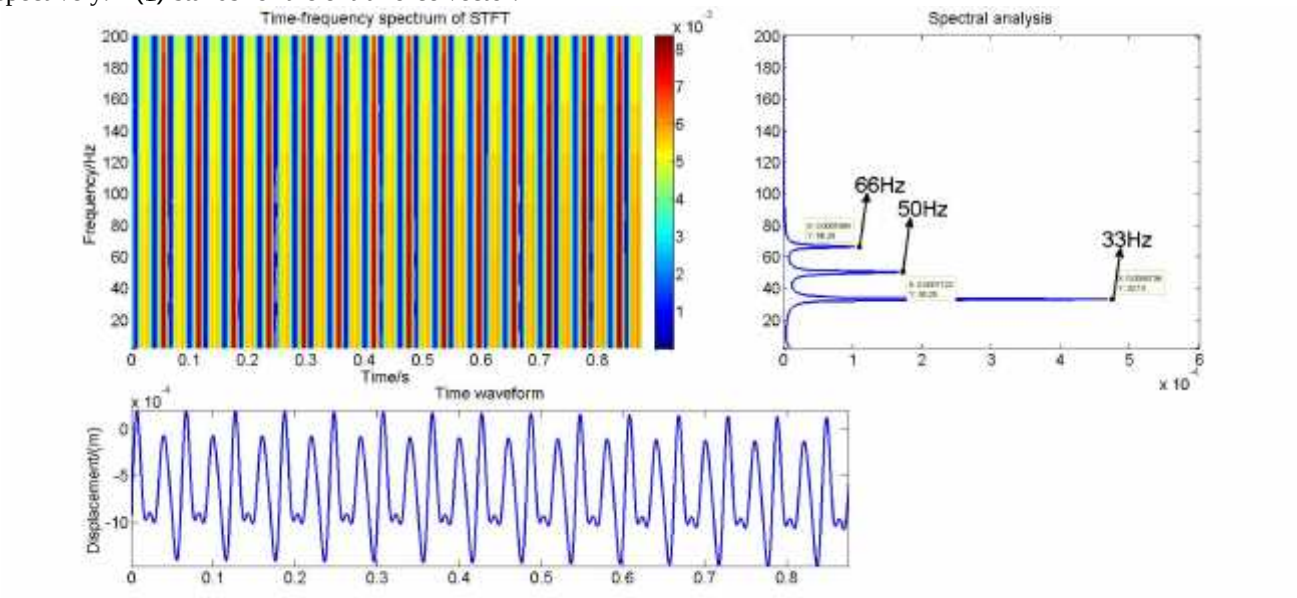

Figure 4 Time-frequency spectrum, time waveform and spectral analysis of the simulation results

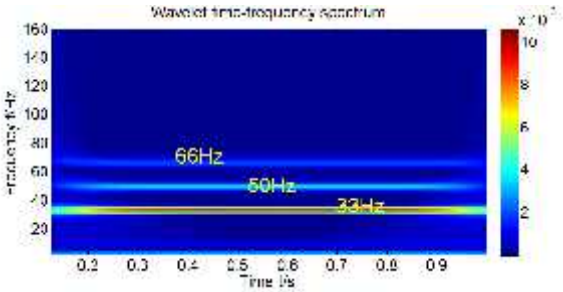

Figure 5 Time-frequency spectrum of wavelet

6 Experimental verification

Experiment are carried out on the dual-rotor system with a centrally mounted disk. In the section the experiment study to detect misalignment from vibration signals is presented. The test dual-rotor setup is as shown in Figure 6.

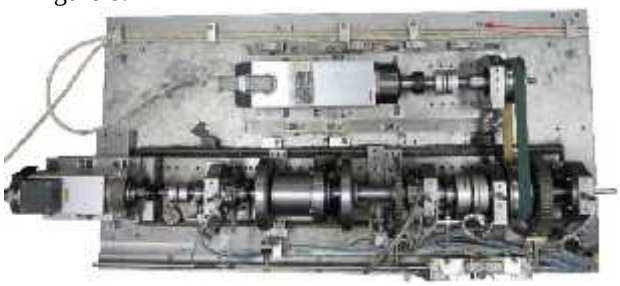

Figure 6 dual-rotor test rig

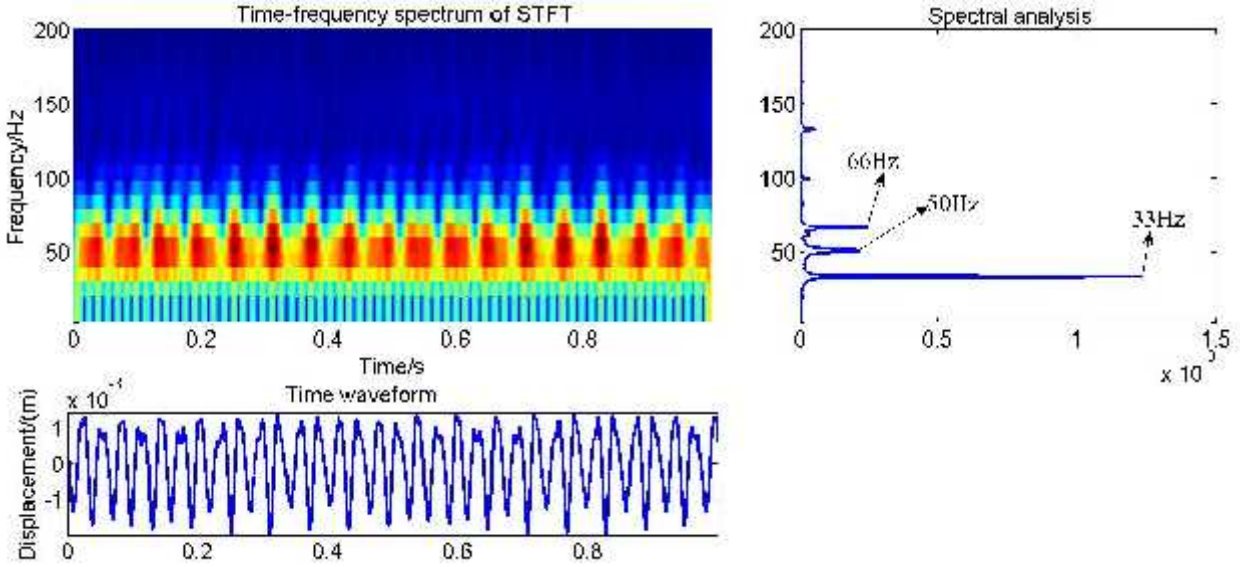

Figure 7 Time-frequency spectrum, time waveform and spectral analysis of the experimental signal

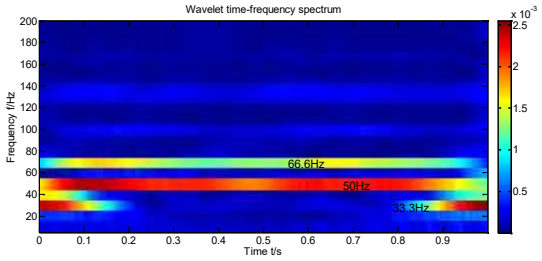

Figure 8 Time-frequency spectrum of wavelet

It can be observed from Figure 7 and Figure 8 that there are three frequency components, in which 33 Hz is the rotation frequency of inner rotor and has the maximum amplitude, while the other two frequency components, respectively, are the rotation frequency of outer rotor and double frequency of inner rotor, which are consistent with the numerical results. According to rotor vibration theory, prominent rotation frequency means the eccentricity of rotor, apparently, the eccentricity results from the imbalance of the screw. Meanwhile, 66 Hz is the double frequency of inner rotor, which demonstrates the misalignment existence of inner rotor.

7 Conclusion

A dynamic model for researching the unbalance-misalignment coupling faults of dual-rotor system with inter-shaft bearing is established in the paper. The vibration characteristics of outer and inner rotors are revealed when the dual-rotor with unbalance-misalignment coupling faults by numerical analysis and experiments. Since the time-frequency resolution of STFT is fixed when the window function and its length are chosen. the time-frequency map of CWT has better performance on extracting misalignment fault characteristics.

Acknowledgements

The support for this research under National Natural Science Foundations of China (No. 11572167) is gratefully acknowledged. The authors are grateful to the editor and anonymous reviewers for their valuable comments.

References

1. J. Piotrowski, Shaft Alignment Handbook, Dekker, New York, 1986.
2. M. Xu, R.D. Marangoni, Vibration analysis of a motor-flexible coupling-rotor system subject to misalignment and unbalance, Part I: Theoretical model and analysis, J. Sound Vib. 176 (1994) 663–679.
3. D.L. Dewell, L.D. Mitchell, Detection of a misaligned disk coupling using spectrum analysis, Trans. ASME J. Vib. Acoust. Stress Reliab. Des. 106 (1984) 9 – 16.
4. M. Xu, R.D. Marangoni, Vibration analysis of a motor-flexible coupling-rotor system subject to misalignment and unbalance, Part II: Experimental validation, J. Sound Vib. 176 (1994) 681–691.
5. N. Hamzaoui, C. Boisson, C. Lesueur, Vibro-acoustic analysis and identification of defects in rotating machinery, Part I: Theoretical model, J. Sound Vib. 216 (1998) 553–570.
6. A.S. Sekhar, B.S. Prabhu, Effects of coupling misalignment on vibrations of rotating machinery, J. Sound Vib. 185 (1995) 655–671.
7. Y.-S. Lee, C.-W. Lee, Modelling and vibration analysis of misaligned rotor-ball bearing systems, J. Sound Vib. 224 (1999) 17–32.
8. N. Bachschmid, P. Pennacchi, A. Vania, Identification of multiple faults in rotor systems, J. Sound Vib. 254 (2002) 327–366.
9. P. Pennacchi, A. Vania, Diagnosis and model based identification of a coupling misalignment, Shock Vib. 12 (2005) 293–308.
10. P. Pennacchi, N. Bachschmid, A. Vania, G.A. Zanetta, L. Gregori. Use of modal representation for the supporting structure in model-based fault identification of large rotating machinery: Part I – Theoretical remarks, Mech. Syst. Signal Process. 20 (2006) 662–681.
11. J.K. Sinha, A.W. Lees, M.I. Friswell, Estimating unbalance and misalignment of a flexible rotating machine from a single rundown, J. Sound Vib. 272 (2004) 967–989.
12. Fei Z X, Tong S G, Wei C. Investigation of the dynamic characteristics of a dual rotor system and its start-up simulation based on finite element method [J]. Journal of Zhejiang University-SCIENCE A, 2013, 14(4):268-280.
13. Feng Z, Liang M, Chu F. Recent advances in time–frequency analysis methods for machinery fault diagnosis: A review with application examples [J]. Mechanical Systems & Signal Processing, 2013, 38(1):165-205.
14. Yan R, Gao R X, Chen X. Wavelets for fault diagnosis of rotary machines: A review with applications[J]. Signal Processing, 2014, 96(5):1–15.
15. Sinha J K. Higher Order Spectra for Crack and Misalignment Identification in the Shaft of a Rotating Machine [J]. Structural Health Monitoring, 2007, 6(4):325-334